Light-pollution model for cloudy and cloudless night skies with ground-based light sources

Miroslav Kocifaj

The scalable theoretical model of light pollution for ground sources is presented. The model is successfully employed for simulation of angular behavior of the spectral and integral sky radiance and/or luminance during nighttime. There is no restriction on the number of ground-based light sources or on the spatial distribution of these sources in the vicinity of the measuring point (i.e., both distances and azimuth angles of the light sources are configurable). The model is applicable for real finite-dimensional surface sources with defined spectral and angular radiating properties contrary to frequently used point-source approximations. The influence of the atmosphere on the transmitted radiation is formulated in terms of aerosol and molecular optical properties. Altitude and spectral reflectance of a cloud layer are the main factors introduced for simulation of cloudy and/or overcast conditions. The derived equations are translated into numerically fast code, and it is possible to repeat the entire set of calculations in real time. The parametric character of the model enables its efficient usage by illuminating engineers and/or astronomers in the study of various light-pollution situations. Some examples of numerical runs in the form of graphical results are presented.

OCIS codes: 010.1290, 290.1090, 290.1310.

1. Introduction

Light pollution became important in the past few decades, especially in highly industrialized and densely populated areas such as in the United States, Japan, and Europe.[1] Light pollution is to be surely understood as a side effect of industrial civilization and urbanization of vast territories. Excessive use of light (overillumination) unnecessarily wastes energy and almost prohibits professional astronomical observations.[2] Scattered nightlight also has perturbing influence on the human life of city residents. Since a human system of visual perception responds efficiently to the short-wave radiation, many instruments measuring light pollution are designed for the visible spectral range.[3] The attenuation of short-wave radiation is related mainly to four individual processes: molecular absorption, molecular scattering, aerosol absorption, and aerosol scattering. Nevertheless, the instability of angular behavior of the scattered light is caused predominately by variation of the scattering pattern of ambient aerosols. Therefore, it is necessary take into account both optical properties of aerosol ensembles and the pure molecular atmosphere[4] when evaluating the spatial characteristics of light pollution in the turbid environment.

Interest in the protection of the night sky from light pollution is continuously growing. Information on light pollution is important not only for astronomers, but also for illuminating engineers who urgently need the approximate, but physically well-justified solution of the light-pollution problem (especially for overcast situations[5]). This paper presents the model that is appropriate for illuminating engineering as it is scalable, numerically fast, and applicable in the calculation of the angular distribution of the diffuse light produced by various types of ground-based sources. Contrary to other approaches,[4,6–7] the model presented in this paper is designed for realistically shaped surface sources and for cloudy skies. The overcast situations were not analyzed in detail until now, since the main attention in light-pollution studies was paid to astronomical observations (which are typically realized under cloudless conditions[8]). A further advantage of the presented model is an easy embedding of any other light source [such as moonlight—see Eq. (25)] into a physical model (and numerical scheme).

The model is applicable in the calculation of spectral and integral radiance or luminance under arbi-

The author (kocifaj@savba.sk) is with ICA SAS, Slovak Academy of Sciences, Dúbravská cesta 9, 845 03 Bratislava, Slovak Republic.

Received 23 October 2006; revised 30 December 2006; accepted 18 January 2007; posted 24 January 2007 (Doc. ID 76363); published 1 May 2007.

0003-6935/07/153013-10$15.00/0

trary atmospheric conditions (cloudy skies inclusive). Theoretical derivations are presented in Section 2. Examples of numerical simulations (Section 3) were performed for cloudless and overcast skies assuming two light sources were situated in the vicinity of the observation point.

2. Theoretical Model of Spectral and Integral Night-Sky Radiance and Luminance

Let us assume an infinitesimal ground area A_0, emitting radiation into the upward hemisphere (Fig. 1). Elementary spectral radiant flux $d\phi_{\lambda,0}$ (W nm^{-1}) through a Lambertian surface can be expressed by means of the intensity $I_\lambda(z_0, \varphi_0)$ [power per unit solid angle per unit projected source area (W m^{-2} nm^{-1} sr^{-1})] as follows:

$$d\phi_{\lambda,0} = A_0 I_\lambda(z_0,\ \varphi_0)\cos z_0 d\omega_0, \tag{1}$$

where z_0 and φ_0 are the zenith and azimuth angles characterizing the direction of light propagation and $d\omega_0 = \sin z_0 dz_0 d\varphi_0$ is the elementary solid angle. While $I_\lambda(z_0, \varphi_0)$ usually shows a weak dependence on φ_0, it varies quite rapidly with z_0. Therefore the radiative flux measured at a distance r_0 is

$$d\phi_{\lambda,0}(h) = d\phi_{\lambda,0} t_\lambda(h,\ z_0) = A_0 I_\lambda(z_0)\cos z_0 \frac{d\sigma_0}{r_0^2} t_\lambda(h,\ z_0). \tag{2}$$

The elementary surface $d\sigma_0$ equals $r_0^2 d\omega_0$, and $t_\lambda(h, z_0)$ is a transmission coefficient,[9] which depends on the optical properties of the atmosphere between the ground and an altitude h [see Eqs. (9a), (9b), and (11)]. The probability that a photon, originally emitted into the solid angle ω_0, will be scattered into a solid angle ω' is characterized by the function:

$$p_\lambda(\omega_0,\ \omega') = \frac{1}{4\pi} P_\lambda(\omega_0,\ \omega')\omega', \tag{3}$$

where $P_\lambda(\omega_0, \omega')$ is the well-known scattering phase function[10] satisfying the normalization condition $\int_{4\pi} P_\lambda(\omega_0, \omega')d\omega' = 4\pi$. The radiant flux directed toward the observer is proportional to the elementary volume $dv_0 = d\sigma_0 dr_0$, and thus

$$d^2\phi^*_\lambda(h,\ z,\ \varphi) = d\phi_{\lambda,0}(h) p_\lambda(\omega_0,\ \omega') k_{sca,\lambda}(h) dr_0, \tag{4}$$

where z is the zenith angle, φ is the azimuth angle of the sky element as seen from the point $\mathcal{P}$ (Fig. 1), and $k_{sca,\lambda}(h)$ is the volume-scattering coefficient characterizing optical properties of the atmosphere at altitude h.[11] The solid angle $\omega' = A/r^2$, where A is the area of a detector and r is the distance between the elementary volume dv_0 and the observer. Let the projection area of dv_0 toward the point $\mathcal{P}$ be $d\sigma$. In such a case $d\sigma_0 dr_0 = dv_0 = d\sigma dr$, so

$$d^2\phi_\lambda(h,\ z,\ \varphi) = A_0 I_\lambda(z_0)\cos z_0 \frac{t_\lambda(h,\ z_0) t_\lambda(h,\ z)}{r_0^2} \times dr k_{sca,\lambda}(h)\left[\frac{A}{4\pi} P_\lambda(\omega_0,\ \omega')\right] d\omega. \tag{5}$$

Here $d\omega = d\sigma/r^2$ is the solid angle subtended by the elementary surface $d\sigma$ at the point $\mathcal{P}$. In accordance with the Beer–Bouguer–Lambert law, the intensity of radiation decreases exponentially with the optical thickness τ_λ,

$$\tau_\lambda(h_1,\ h_2) = \int_{h_1}^{h_2} k_{ext,\lambda}(h')dh', \tag{6}$$

where h_1 and h_2 are the bottom and top altitudes of the atmospheric layer, respectively, and $k_{ext,\lambda}(h')$ is the volume extinction coefficient at the altitude h'.

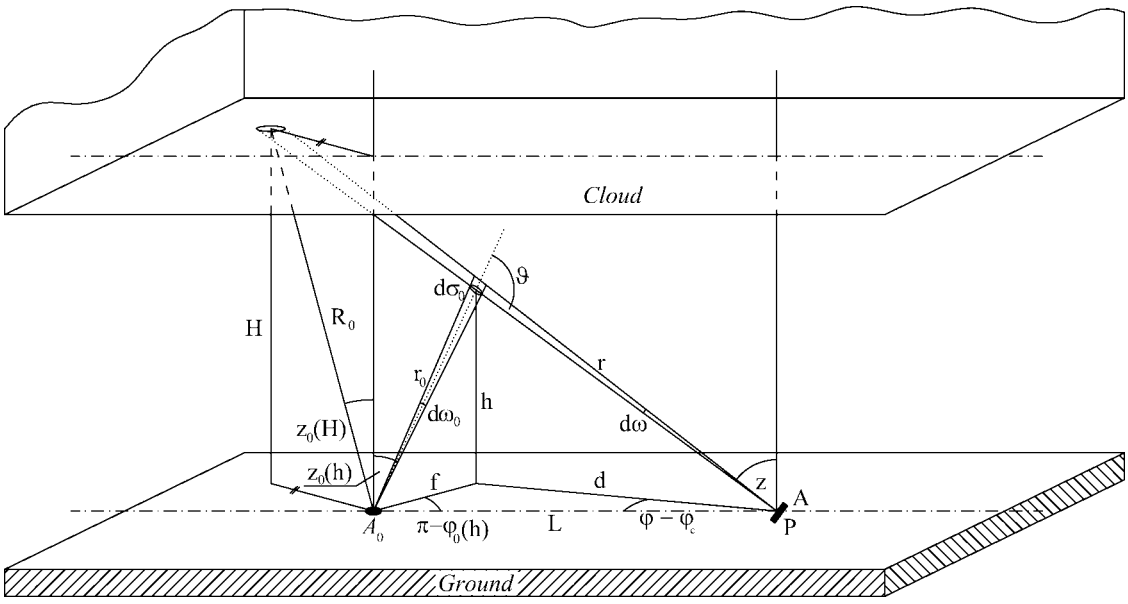

Fig. 1. Geometrical setup of the light-pollution model.

Aerosol particles (A) and air molecules (M) are the most important atmospheric constituents responsible for attenuation of the visible radiation, so it is sufficiently accurate to write

$$k_{ext,\lambda}(h') = k_{ext,\lambda}^{(M)}(h') + k_{ext,\lambda}^{(A)}(h'). \tag{7}$$

Equation (6) for both aerosols and molecules yields

$$\tau_\lambda^{(M)}(0,\ h) = \int_0^h k_{ext,\lambda}^{(M)}(h')\mathrm{d}h', \tag{8a}$$

$$\tau_\lambda^{(A)}(0,\ h) = \int_0^h k_{ext,\lambda}^{(A)}(h')\mathrm{d}h'. \tag{8b}$$

Based on these definitions, the transmission coefficients used in Eq. (5) are

$$t_\lambda(h,\ z_0) = \exp\{-M_\lambda^{(M)}(z_0)\tau_\lambda^{(M)}(0,\ h) - M_\lambda^{(A)}(z_0)\tau_\lambda^{(A)}(0,\ h)\}, \tag{9a}$$

$$t_\lambda(h,\ z) = \exp\{-M_\lambda^{(M)}(z)\tau_\lambda^{(M)}(0,\ h) - M_\lambda^{(A)}(z)\tau_\lambda^{(A)}(0,\ h)\}, \tag{9b}$$

where $M_\lambda^{(M)}(z)$ and $M_\lambda^{(A)}(z)$ are the relative molecular and aerosol optical air masses, respectively. However, the values of $M_\lambda^{(M)}$ and $M_\lambda^{(A)}$ differ practically only in the region of the horizon.[12]

The geometry of the problem shows that the zenith angle z_0 changes with both the direction of the observation (z, φ) and the altitude h (Fig. 1). If L is a horizontal distance of the elementary area A_0 from point $\mathcal{P}$, and φ_C is an azimuth angle of A_0 measured in $\mathcal{P}$, one can obtain

$$\cos z_0(h,\ z,\ \varphi) = \left\{\left(1 + tg^2 z\right) + \frac{L}{h} \times \left[\frac{L}{h} - 2tgz\,\cos(\varphi - \varphi_C)\right]\right\}^{-1/2}. \tag{10}$$

We adopt the convention $z_{0,h} \equiv z_0(h, z, \varphi)$ [or $z_{0,H} \equiv z_0(H, z, \varphi)$] to avoid complexities in further formulas. It is practical to introduce an overall transmission function:

$$T_\lambda(h,\ z,\ \varphi) = t_\lambda(h,\ z)t_\lambda(h,\ z_{0,h}). \tag{11}$$

We have written $T_\lambda(h, z, \varphi)$ instead of $T_\lambda(h, z)$ formally, since $z_{0,h}$ is a function of φ [we refer to Eq. (10)]. Whereas $r_0 = h/\cos z_{0,h}$ and $\mathrm{d}r = \mathrm{d}h/\cos z$, Eq. (5) translates into

$$\mathrm{d}^2\phi_\lambda(h,\ z,\ \varphi) = A_0 I_\lambda(z_{0,h})\cos^3 z_{0,h}\,\frac{T_\lambda(h,\ z,\ \varphi)}{h^2}\,\frac{\mathrm{d}h}{\cos z} \times \left[\frac{A}{4\pi}\,k_{sca,\lambda}(h)P_\lambda(\omega_0,\ \omega')\right]\mathrm{d}\omega. \tag{12}$$

The product of $k_{sca,\lambda}(h)$ and $P_\lambda(\omega_0, \omega')$,

$$k_{sca,\lambda}(h)P_\lambda(\omega_0,\ \omega') = k_{sca,\lambda}^{(M)}(h)P_\lambda^{(M)}(\omega_0,\ \omega') + k_{sca,\lambda}^{(A)}(h)P_\lambda^{(A)}(\omega_0,\ \omega'), \tag{13}$$

reflects the optical properties of the elementary volume of molecular-aerosol atmosphere. Direction of propagation of the scattered light is characterized by ω' (in a symbolic way). Introducing the scattering angle ϑ,[11] the phase function for molecular scattering can be expressed analytically

$$P_\lambda^{(M)}(\omega_0,\ \omega') \equiv P_\lambda^{(M)}(\vartheta) = \tfrac{3}{4}\left(1 + \cos^2\vartheta\right), \tag{14}$$

while the aerosol phase function $P_\lambda^{(A)}(\omega_0, \omega')$ is quite complex and usually can only be obtained numerically.[13] Although the Henyey–Greenstein function[10]

$$P_\lambda^{(A)}(\omega_0,\ \omega') \equiv P_\lambda^{(A)}(\vartheta) = \frac{\left(1 - g_\lambda^2\right)}{\left(1 + g_\lambda^2 - 2g_\lambda^2\cos\vartheta\right)^{3/2}} \tag{15}$$

is often used in aerosol modeling,[14,15] it may not be appropriate to simulate the phase function for irregularly shaped dust grains.[16] The asymmetry parameter g_λ in Eq. (15) is the cosine-weighted integral of the aerosol-scattering phase function. It is a single value that describes the angular scattering of aerosols that is computationally efficient for radiative transfer modeling. The scattering angle ϑ_λ at the altitude h is

$$\cos\vartheta_h = \frac{1}{2}\left(\frac{L^2}{h^2}\cos z\,\cos z_{0,h} - \frac{\cos z_{0,h}}{\cos z} - \frac{\cos z}{\cos z_{0,h}}\right) \tag{16}$$

according to the geometry presented in Fig. 1. Finally, the radiation flux due to the scattering in the cloud-free atmosphere is

$$\mathrm{d}^2\phi_\lambda(h,\ z,\ \varphi) = A_0 A I_\lambda(z_{0,h})\cos^3 z_{0,h}\,\frac{T_\lambda(h,\ z,\ \varphi)}{h^2} \times \Gamma_\lambda(h,\ z,\ \varphi)\frac{\mathrm{d}h}{\cos z}\,\mathrm{d}\omega, \tag{17}$$

where

$$\begin{aligned}\Gamma_\lambda(h,\ z,\ \varphi) &= \frac{1}{4\pi}\left[k_{sca,\lambda}^{(M)}(h)P_\lambda^{(M)}(\omega_0,\ \omega') + k_{sca,\lambda}^{(A)}(h)P_\lambda^{(A)}(\omega_0,\ \omega')\right] \\ &= \frac{1}{4\pi}\left[\Omega_\lambda^{(M)}k_{ext,\lambda}^{(M)}(h)P_h^{(M)}(\omega_0,\ \omega') + \Omega_\lambda^{(A)}k_{ext,\lambda}^{(A)}(h)P_\lambda^{(A)}(\omega_0,\ \omega')\right]\end{aligned} \tag{18}$$

characterizes an angular distribution of the light scattered at the altitude h and $\Omega_\lambda^{(A)}$ is the single-

scattering albedo of aerosol particles[17] (note that molecular single-scattering albedo $\Omega_\lambda^{(M)} = 1$).

Using Eq. (2) for radiative flux reaching a cloud at altitude H and employing $R_0 = H/\cos z_{0,H}$, the radiant flux directed from the cloud toward the observer is

$$\begin{aligned} \mathrm{d}\phi_{\lambda,1}^{*}(H) &= \mathrm{d}\phi_{\lambda,0}(H)\cos z_{0,H}\rho_\lambda(z_{0,H},\ z,\ \vartheta_H) \\ &= A_0 I_\lambda(z_{0,H})\rho_\lambda(z_{0,H},\ z,\ \vartheta_H)\cos^4 z_{0,H}\,\frac{\mathrm{d}\sigma_0}{H^2} \\ &\quad \times t_\lambda(H,\ z_{0,H}), \end{aligned} \tag{19}$$

where $\rho_\lambda(z_{0,H}, z, \vartheta_H)$ is a spectral reflectance of the cloud.[18] The radiative flux in $\mathcal{P}$ is expressed in the form

$$\begin{aligned} \mathrm{d}\phi_{\lambda,0}(H,\ z,\ \varphi) &= A_0 I_\lambda(z_{0,H})\cos^4 z_{0,H}\,\frac{\cos z\,\mathrm{d}\sigma_0}{H^2} \\ &\quad \times T_\lambda(H,\ z,\ \varphi)\frac{A\rho_\lambda(z_{0,H},\ z,\ \vartheta_H)}{\pi r^2}, \end{aligned} \tag{20}$$

where the solid angle ω' was replaced by the ratio A/r^2 (r is a distance from the radiating elementary area of the cloud to the observer) and ϑ_H is expressed by Eq. (16) (using $z_{0,H}$ instead of $z_{0,h}$). Whereas

$$\mathrm{d}\omega = \frac{\cos z\,\mathrm{d}\sigma_0}{\cos z_{0,H} r^2}, \tag{21}$$

the contribution of the cloud to the radiant flux measured by the observer is

$$\begin{aligned} \mathrm{d}\phi_{\lambda,0}(H,\ z,\ \varphi) &= A_0\,\frac{A\rho_\lambda(z_{0,H},\ z,\ \vartheta_H)}{\pi H^2}\,I_\lambda(z_{0,H})\cos^5 z_{0,H} \\ &\quad \times T_\lambda(H,\ z,\ \varphi)\mathrm{d}\omega. \end{aligned} \tag{22}$$

Total intensity is therefore

$$I_\lambda(z,\ \varphi) = \frac{\mathrm{d}\phi_{\lambda,0}(H,\ z,\ \varphi)}{A\mathrm{d}\omega} + \frac{1}{A\mathrm{d}\omega}\int_0^H \mathrm{d}^2\phi_\lambda(h,\ z,\ \varphi), \tag{23}$$

i.e.,

$$\begin{aligned} I_\lambda(z,\ \varphi) &= \frac{A_0\rho_\lambda(z_{0,H},\ z,\ \vartheta_H)}{\pi H^2}\,I_\lambda(z_{0,H})\cos^5 z_{0,H} \\ &\quad \times T_\lambda(H,\ z,\ \varphi) + \frac{A_0}{\cos z}\int_0^H I_\lambda(z_{0,h})\cos^3 z_{0,h} \\ &\quad \times \frac{T_\lambda(h,\ z,\ \varphi)}{h^2}\,\Gamma_\lambda(h,\ z,\ \varphi)\mathrm{d}h. \end{aligned} \tag{24}$$

The contribution of the moonlight to $I_\lambda(z, \varphi)$ can be obtained in agreement with Ref. 9 in the first scattering-order approximation

$$\begin{aligned} I_\lambda^{\text{with } ML}(z,\ \varphi) &= I_\lambda(z,\ \varphi) + \frac{I_\lambda^{ML}}{\cos z}\int_0^H \Gamma_\lambda^{ML}(h,\ z,\ \varphi) \\ &\quad \times [t_\lambda(\infty,\ \xi_0) - t_\lambda(h,\ \xi_0)]t_\lambda(h,\ z)\mathrm{d}h, \end{aligned} \tag{25}$$

where $I_\lambda^{\text{with } ML}(z, \varphi)$ is the total intensity measured by the observer (moonlight inclusive), I_λ^{ML} is the extraterrestrial intensity of the moonlight, ξ_0 is the zenith angle of the Moon, and $\Gamma_\lambda^{ML}(h, z, \varphi)$ is defined the same way as $\Gamma_\lambda(h, z, \varphi)$ [see Eq. (18)] with the exception that the scattering angle $\vartheta = \vartheta^{ML}$ is now calculated as

$$\cos\vartheta^{ML} = \cos\xi_0\cos z + \sin\xi_0\sin z\cos\alpha_0. \tag{26}$$

The quantity α_0 is the azimuth angle of the Moon as seen from $\mathcal{P}$. Calculating $\Gamma_\lambda^{ML}(h, z, \varphi)$, the scattering angle ϑ in Eqs. (14), (15), and (18) must be replaced by the scattering angle ϑ^{ML}. Nevertheless, we will not deal with the moonlight as the aim of the paper is to recognize how the ground-based light sources can influence sky radiances (especially under overcast situation). The moonlight may work as a disturbing factor, which makes the above-discussed analysis impossible.

The first term on the right-hand side of Eq. (24) represents a contribution of the cloud to the total intensity, while the second term corresponds to scattering in the cloud-free atmosphere. Garstang[19,20] found an approximate formula $B(Q, q, z_0) = 2Q(1 - q)\cos z_0 + 0.554qz_0^4$ for angular behavior of radiation produced by surface light sources (like cities). His formula can be inserted into our model as follows

$$\begin{aligned} I_\lambda(z,\ \varphi) &= I_{\lambda,0}\,\frac{A_0\rho_\lambda(z_{0,H},\ z,\ \vartheta_H)}{\pi H^2}\cos^4 z_{0,H}B(Q,\ q,\ z_{0,H}) \\ &\quad \times T_\lambda(H,\ z,\ \varphi) \\ &\quad + \frac{A_0 I_{\lambda,0}}{\cos z}\int_0^H B(Q,\ q,\ z_{0,h})\cos^2 z_{0,h} \\ &\quad \times \frac{T_\lambda(h,\ z,\ \varphi)}{h^2}\,\Gamma_\lambda(h,\ z,\ \varphi)\mathrm{d}h. \end{aligned} \tag{27}$$

The quantity Q is the fraction of the light that is isotropically reflected from the ground, and q is the fraction radiated directly into the upward hemisphere. Let the measuring point be surrounded by N light sources, where the radiative characteristics of the ith source are $I_{0,i}$, Q_i, q_i, and the distance and the azimuth of the ith source are L_i and $\varphi_{C,i}$, respectively. The total monochromatic intensity of the scattered light is calculated as a sum over all

sources:

$$J_\lambda(z,\ \varphi) = \sum_{i=1}^{N} I_{\lambda,i}(z,\ \varphi). \tag{28}$$

Nevertheless, the standard detectors operate over a finite spectral band $\langle \lambda_1, \lambda_2 \rangle$ rather than in the monochromatic regime. The right-hand side of Eq. (28) must be integrated

$$J(z,\ \varphi) = \sum_{i=1}^{N} \int_{\lambda_1}^{\lambda_2} I_{\lambda,i}(z,\ \varphi)\mathrm{d}\lambda. \tag{29}$$

Inserting spectral luminous efficiency for an individual observer V_λ (Ref. 21) into Eq. (29), we can obtain luminance:

$$J_V(z,\ \varphi) = \sum_{i=1}^{N} \int_{\lambda_1}^{\lambda_2} V_\lambda I_{\lambda,i}(z,\ \varphi)\mathrm{d}\lambda. \tag{30}$$

Equations (27)–(30) were obtained under the assumption that the characteristic size of a light source is sufficiently small in comparison with the altitude of the cloud, i.e., $\sqrt{4A_0/\pi} \lessapprox H/10$. However, this is a seldom case, and therefore the contribution of the ith light source to the spectral radiance must be expressed in the integral form:

$$\begin{aligned} I_{\lambda,i}(z,\ \varphi) = {} & \frac{I_{\lambda,0,i}}{\pi H^2} \int_{R=0}^{R_i(\varphi_0')} \int_{\varphi_0'=0}^{2\pi} \rho_\lambda(z_{0,H,i},\ z,\ \vartheta_{H,i}) \cos^4 z_{0,H,i} \\ & \times B(Q_i,\ q_i,\ z_{0,H,i}) T_\lambda(H,\ z,\ \varphi) \sin\varphi_0' \mathrm{d}\varphi_0' \mathrm{d}R \\ & + \frac{I_{\lambda,0,i}}{\cos z} \int_0^{R_i(\varphi_0')} \int_{\varphi_0'=0}^{2\pi} \int_0^{H} B(Q_i,\ q_i,\ z_{0,h,i}) \\ & \times \cos^2 z_{0,h,i}\, \frac{T_\lambda(h,\ z,\ \varphi)}{h^2} \\ & \times \Gamma_\lambda(h,\ z,\ \varphi)\mathrm{d}h \sin\varphi_0' \mathrm{d}\varphi_0' \mathrm{d}R, \end{aligned} \tag{31}$$

where index i was added to the quantities depending on one of the following characteristics of the ith light source: $I_{0,i}$, Q_i, q_i, L_i, or $\varphi_{C,i}$. In general, a pattern of a town could be arbitrary, so we use $R_i(\varphi_0')$ for the radial coordinate as a function of the polar angle of the ith city. The position of any elementary area of the city is given by a position vector R (measured from the center of the city) and polar angle φ_0', which determines an orientation of the position vector R (Fig. 1). Equa-

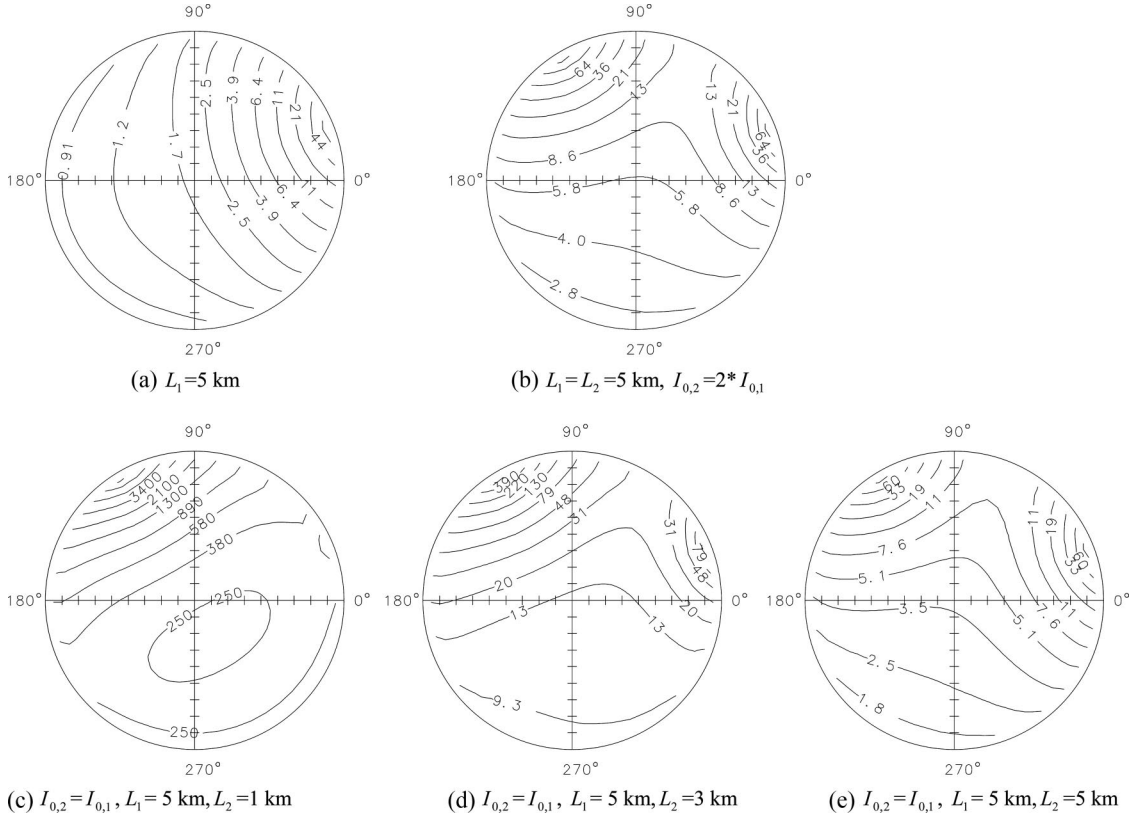

Fig. 2. Distribution of integral radiances under cloudless conditions. The angle along the circle represents azimuth of the sky element. The zenith angle of the element is measured from the center to the margin of the polar graph. (a) L_1 = 5 km, (b) $L_1 = L_2$ = 5 km, $I_{0,2}$ = 2 * $I_{0,1}$, (c) $I_{0,2} = I_{0,1}$, L_1 = 5 km, L_2 = 1 km, (d) $I_{0,2} = I_{0,1}$, L_1 = 5 km, L_2 = 3 km, (e) $I_{0,2} = I_{0,1}$, L_1 = 5 km, L_2 = 5 km.

tion (30) for the ith city is

$$J_{V,i}(z,\ \varphi) = \frac{1}{\pi H^2}\int_{R=0}^{R_i(\varphi_0')}\int_{\varphi_0'=0}^{2\pi}\cos^4 z_{0,H,i}B(Q_i,\ q_i,\ z_{0,H,i}) \times\left\{\int_{\lambda_1}^{\lambda_2}\rho_\lambda(z_{0,H,i},\ z,\ \vartheta_{H,i})I_{\lambda,0,i}V_\lambda \times T_\lambda(H,\ z,\ \varphi)\mathrm{d}\lambda\right\}\sin\varphi_0'\mathrm{d}\varphi_0'\mathrm{d}R + \frac{1}{\cos z} \times\int_{R=0}^{R_i(\varphi_0')}\int_{\varphi_0'=0}^{2\pi}\int_0^H B(Q_i,\ q_i,\ z_{0,h,i})\frac{\cos^2 z_{0,h,i}}{h^2} \times\left\{\int_{\lambda_1}^{\lambda_2} I_{\lambda,0,i}V_\lambda T_\lambda(h,\ z,\ \varphi)\Gamma_\lambda(h,\ z,\ \varphi)\mathrm{d}\lambda\right\} \times \mathrm{d}h\ \sin\varphi_0'\mathrm{d}\varphi_0'\mathrm{d}R. \quad (32)$$

In the case of a circular pattern of a town, the boundary value of R does not depend on the polar angle φ_0' [i.e., $R(\varphi_0') = R_{\max}$]. We highlight that Eq. (10) cannot be used for the surface light source. Instead, the following equations:

$$tg^2 z_{0,h,i}(h,\ z,\ \varphi) = tg^2 z + \frac{R^2 + L_i^2 + 2RL_i\cos\varphi_0'}{h^2} - \frac{2tgz}{h}[(L_i + R\cos\varphi_0')\cos(\varphi - \varphi_{C,i}) + R\sin(\varphi - \varphi_{C,i})\sin\varphi_0'], \quad (33)$$

must be applied for the ith city. The presented theory can also be used for partly cloudy skies. However, this case can be solved only numerically, because of complex geometrical configurations (e.g., spatial distribution or shapes of the clouds). In principle, the integration in the second term of Eq. (27) can be realized only in cloud-free sky windows. The contribution of the reflected light [the first term in Eq. (27)] depends on the shape of a cloud. Whenever the projected areas associated with cosines of z and z_0 [see Eqs. (19)–(22)] need to be adapted, Earth's ground and a surface of the cloud are not plan parallel. The projection area at a cloud surface changes with the orientation of the normal vector to the surface. The numerical implementation of the model must be enhanced to accept these geometrical relations.

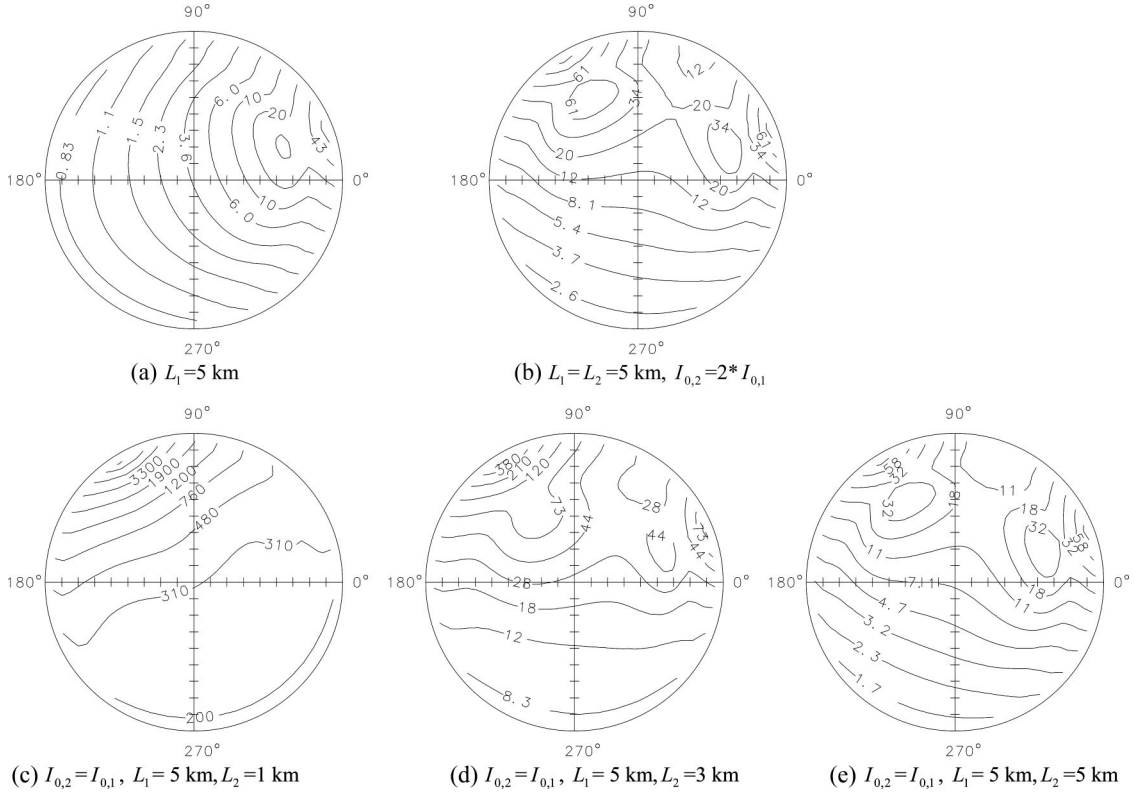

Fig. 3. Distribution of integral radiances in the case of overcast sky (H = 1 km, $\bar{\rho}$ = 0.4). The angle along the circle represents azimuth of the sky element. The zenith angle of the element is measured from the center to the margin of the polar graph. (a) L_1 = 5 km, (b) $L_1 = L_2$ = 5 km, $I_{0,2} = 2 * I_{0,1}$, (c) $I_{0,2} = I_{0,1}$, L_1 = 5 km, L_2 = 1 km, (d) $I_{0,2} = I_{0,1}$, L_1 = 5 km, L_2 = 3 km, (e) $I_{0,2} = I_{0,1}$, L_1 = 5 km, L_2 = 5 km.

3. Numerical Demonstration for One and Two Independent Surface Light Sources

The previous section focused on detail derivation of the equations for the light-pollution model. To demonstrate behavior of the model, we simulated some typical situations assuming a set of approximations. In radiative transfer modeling, it is usually assumed that volume extinction coefficient for molecular atmosphere $k_{ext,\lambda}^{(M)}(h)$ decreases exponentially with the altitude,[22] i.e., $\tau_\lambda^{(M)}(0, h) = \tau_{\lambda,0}^{(M)} f(P, T)[1 - e^{-h/h_0}]$. Here h_0 is a scale height[23] (i.e., the altitude up to which a homogeneous molecular atmosphere would extend), $\tau_{\lambda,0}^{(M)}$ is the molecular optical thickness of the whole atmosphere, and $f(P, T)$ is a function that accounts for the dependency of $\tau_\lambda^{(M)}(0, h)$ on the atmospheric pressure and temperature at height h. We have omitted the function $f(P, T)$ in numerical runs (because it influences the calculated sky radiances at the ground only slightly—especially under overcast conditions). In agreement with Ref. 11, the $\tau_\lambda^{(A)}(0, \lambda)$ reads

$$\tau_\lambda^{(A)}(0,\ h) = \tau_{\lambda,0}^{(A)}\left[1 - e^{-\gamma h}\right], \tag{34}$$

where γ is a vertical gradient of concentration of aerosol particles and $\tau_{\lambda,0}^{(A)}$ is aerosol optical thickness of the whole atmosphere. As the numerical simulations were realized for $z < 85°$, we approximated any optical mass by the formula $M(z) \cong 1/\cos z$. Taking this fact and Eq. (34) into account, we modify Eqs. (11) and (18) to

$$T_\lambda(h,\ z,\ \varphi) = \exp\left\{\left[\frac{1}{\cos z_{0,h}} + \frac{1}{\cos z}\right]\left[\tau_{\lambda,0}^{(M)}\left(e^{-h/h_0} - 1\right) + \tau_{\lambda,0}^{(A)}\left(e^{-\gamma h} - 1\right)\right]\right\}, \tag{35}$$

$$\Gamma_\lambda(h,\ z,\ \varphi) = \frac{1}{4\pi}\left[\Omega_\lambda^{(M)} P_\lambda^{(M)}(\vartheta)\frac{\tau_{\lambda,0}^{(M)}}{h_0}\, e^{-h/h_0} + \Omega_\lambda^{(A)} P_\lambda^{(A)}(\vartheta)\gamma\tau_{\lambda,0}^{(A)} e^{-\gamma h}\right]. \tag{36}$$

In general, the spectral reflectance of the cloud ρ_λ depends on $z_{0,H}$, z, and ϑ_H.[24] However, the approximation $\rho_\lambda(z_{0,H}, z, \vartheta_H) \cong \rho_\lambda$ (Ref. 25) is usually satisfactory for illuminating engineer purposes.[5]

In numerical runs, the source of light is assumed to be negligibly small in comparison with both the altitude of the clouds and the distance to the observer. At first, we analyzed the situation when only one light source was present in a fixed position in the vicinity of the measuring point ($L_1 = 5$ km, and $\varphi_{C,1} = 20°$). In the next example, an additional light source of the same radiating properties as the first one was positioned at $\varphi_{C,2} = 120°$. The distance L_2 to the second source varied from 1 to 5 km. We paid attention especially to a situation when both sources are equally distant ($L_1 = L_2 = 5$ km), but the power of the second

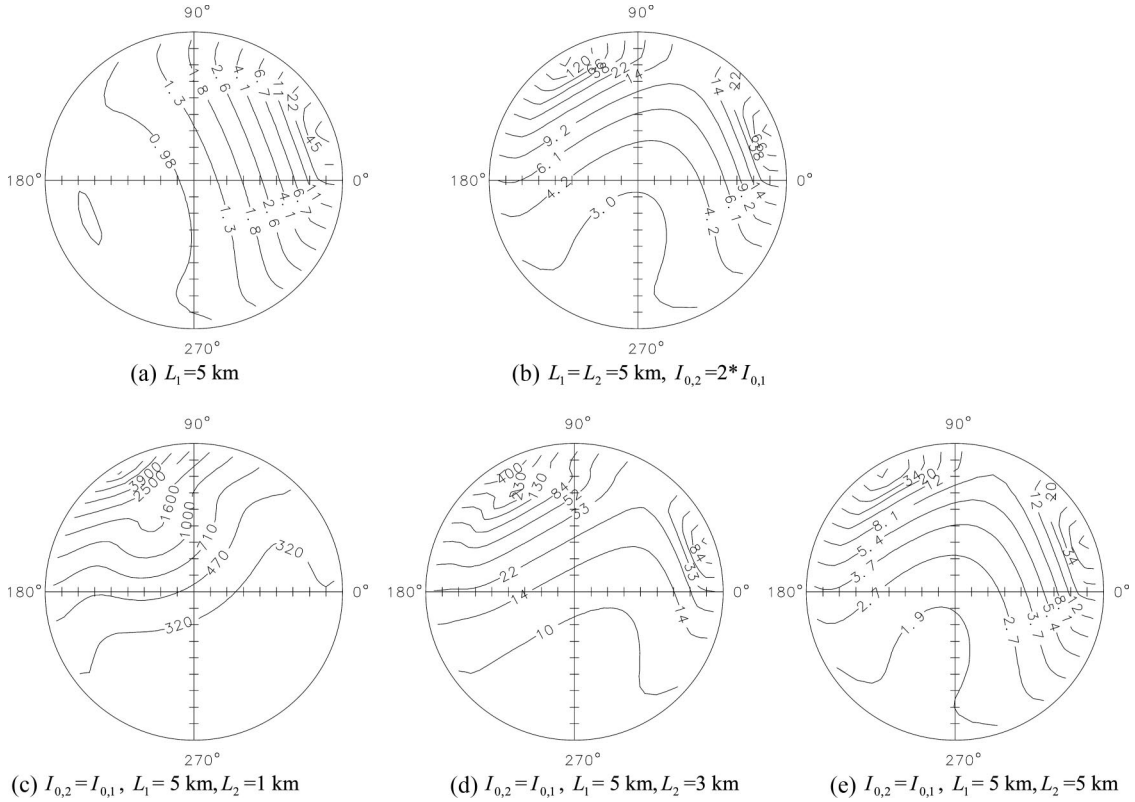

Fig. 4. Distribution of integral radiances under overcast conditions (H = 1 km, $\bar{\rho}$ = 0.7). The rest description of the figure is the same as in Fig. 3.

source is approximately two times the power of the first source. The physical characteristics applied in numerical runs are: $h_0 = 8$ km, $\gamma = 0.65\ \mathrm{km}^{-1}$, $g_\lambda = 0.90$, $\Omega_\lambda^{(A)} = 0.85$, $\Omega_\lambda^{(M)} = 1.0$, $Q = 0.15$, $q = 0.15$. To obtain sufficiently comprehensive results and to make their interpretation straightforward, we accepted these conditions: $V_\lambda \equiv 1.0$, $I_{\lambda,0} \equiv 1.0$, $A_0 \equiv 1.0$, $\rho_\lambda \equiv \bar{\rho}$. Numerical simulations cover the spectral band $\lambda \in \langle 0.45, 0.75\ \mu\mathrm{m} \rangle$, in which the molecular and aerosol optical thicknesses were modeled as: $\tau_{\lambda,0}^{(M)} \sim \lambda^{-4.09}$ and $\tau_{\lambda,0}^{(A)} \sim \lambda^{-1}$ (with a reference aerosol optical thickness $\tau_{\lambda=500\ \mathrm{nm},0}^{(A)} = 0.4$). Green *et al.*[26] have shown that an average reflectance of a cloud is ~0.46, while possibly realizable values of $\bar{\rho}$ can be scattered over a wide range.[24,27,28] To simulate quite different situations, we adopted two values for spectral reflectance: $\bar{\rho} = 0.4$ and $\bar{\rho} = 0.7$, and also two different altitudes of a cloud: $H = 1$ km and $H = 3$ km. Graphical results for polychromatic radiances are presented in relative units (the coefficient of proportionality is 10^6) and the isolines are drawn on a logarithmic scale.

A. Cloudless Conditions

The sky radiances are typically symmetric toward the single source of light in the case of cloudless conditions [Fig. 2(a)]. In addition, spatial behavior of sky radiances is characterized by a steep gradation along angular distance to the source of light (reduction of the intensity may reach 2 orders of magnitude). The presence of a second source of light leads to a deformation of the angular structure of the sky radiances, depending on the mutual relation between geometrical configuration and radiating characteristics of both light sources [Figs. 2(b)–2(e)]. Theoretical isolines of the sky radiances show perfect symmetry around the meridian with azimuth $\varphi = (\varphi_{C,1} + \varphi_{C,2})/2$ if two light sources have the same power, size, and distance to the measuring point $\mathcal{P}$ [Fig. 2(e)]. The absolute values of the sky radiances may increase in ~2 orders of magnitude when a light source approaches from 5 to 1 km.

B. Overcast Sky

The presence of low clouds ($H < 2$ km) is, in principle, accompanied with the sharpening of a limb around the source of light (Figs. 3 and 4). An appearance of light effects similar to light pillars can occur when the light source is situated near the measuring point [Fig. 3(c)]. The probability of the occurrence of such optical effects grows as the cloud reflectance increases [see, e.g., Figs. 4(c) and 4(d)]. The influence of the clouds on spatial distribution of sky radiances evidently diminishes as the altitude of the clouds H grows. As for overcast conditions: the combined contribution of scattering in a cloud-free atmosphere and reflection by the clouds may lead to pre-exposure of the light at elevated angles above the light source [Figs. 5(e), 6(a), 6(b), 6(d), 6(e)]. It deals predominately with sky elements positioned at the light-source meridian with zenith angle $z_{\max} \approx \arctan(L/H)$, where L is the

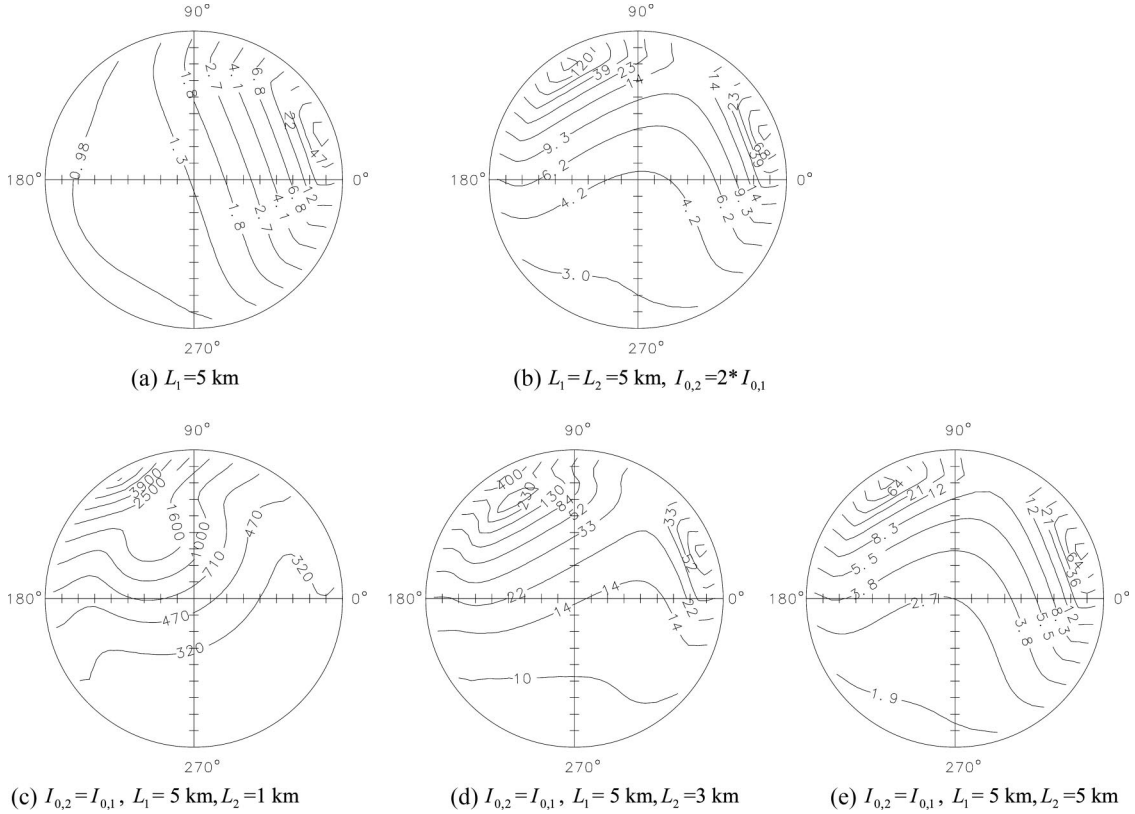

Fig. 5. Distribution of integral radiances under overcast conditions ($H = 3$ km, $\bar{\rho} = 0.4$). The rest description of the figure is the same as in Fig. 3.

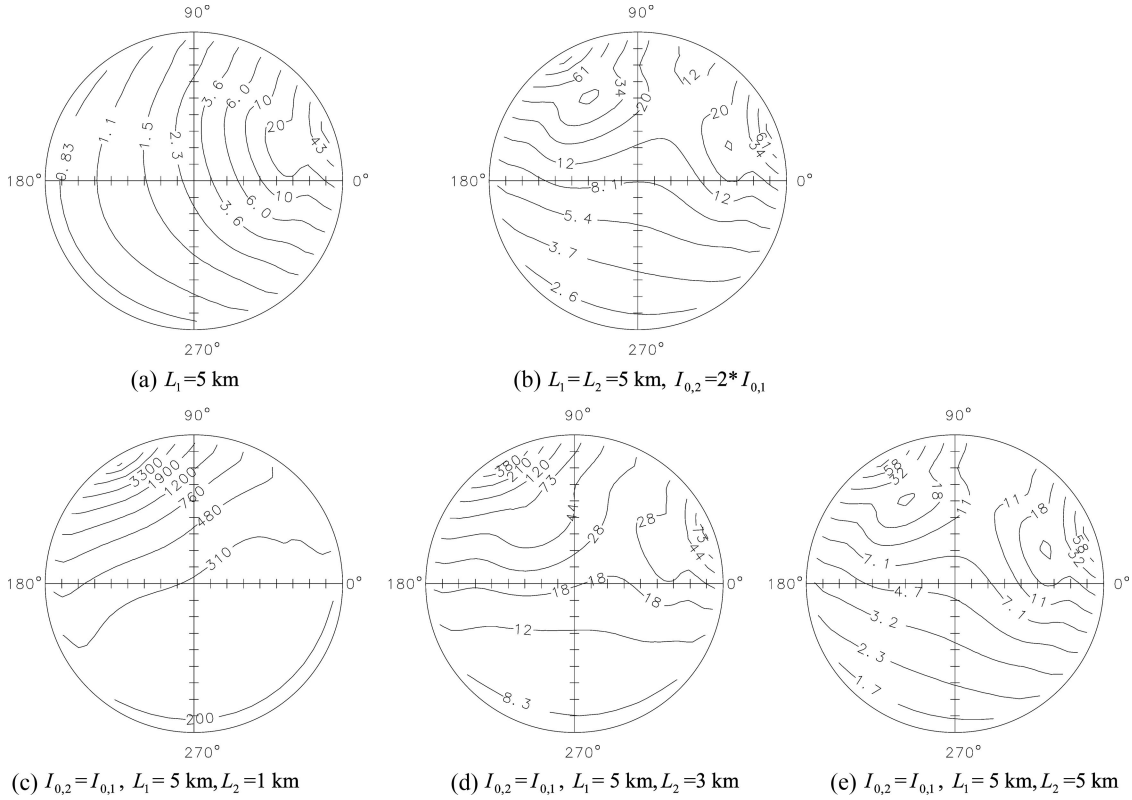

(a) L_1=5 km (b) $L_1=L_2$=5 km, $I_{0,2}=2*I_{0,1}$

(c) $I_{0,2}=I_{0,1}$, L_1= 5 km, L_2=1 km (d) $I_{0,2}=I_{0,1}$, L_1= 5 km, L_2=3 km (e) $I_{0,2}=I_{0,1}$, L_1= 5 km, L_2=5 km

Fig. 6. Distribution of integral radiances under overcast conditions (H = 3 km, $\bar{\rho}$ = 0.7). The rest description of the figure is the same as in Fig. 3.

distance between the light source and the observer. Therefore the most significant contribution to the light excess at $z_{\max}$ originates from clouds situated just in the zenith of the ground-based light source [Figs. 5(b), 5(c) and 6(a), 6(b), 6(d), 6(e) for middle clouds). The greater reflectance, the more obvious light excess can be expected (compare Figs. 5 and 6).

4. Concluding Remarks

A successful theoretical solution was derived for night-sky radiances (and luminance). The solution enables very fast and sufficiently accurate numerical calculations of spectral and/or integral sky radiances under cloudless, cloudy, and overcast conditions. Compared with point-source approximations (the most frequently employed approach), the presented model deals with the spectral radiant fluxes (and flux densities) and thus, makes possible numerical simulations for finite-dimensional light sources. To illustrate the angular behavior of the integral (polychromatic) sky radiances under different conditions, the results of demonstrational numerical runs are summarized in Section 3. It was shown that light pillars can occur under cloudy conditions when a ground-based light source is situated near the measuring point. The presence of such optical effects was not confirmed in a cloud-free atmosphere. On the other hand, pre-exposure of the light can be observed in the sky above the light source in the case of overcast skies. The most significant contribution to the light excess originated from clouds situated just in the zenith of the light source. Experimental verification of the theoretical results is ongoing (it is solved within Ref. 5 and also as a part of the a project (Ref. 29).

This work was supported by the Scientific Grant Agency VEGA (grant 2/5093/5).

References

1. A. Barducci, P. Marcoionni, I. Pippi, and M. Poggesi, "Effects of light pollution revealed during a nocturnal aerial survey by two hyperspectral imagers," Appl. Opt. **42,** 4349–4361 (2003).
2. P. Cinzano and C. D. Elvidge, "Night sky brightness at sites from DMSP-OLS satellite measurements," Mon. Notes Astron. Soc. **353,** 1107–1116 (2004).
3. P. Cinzano, "A portable spectrophotometer for light pollution measurements," Mem. Soc. Astron. Ital. Suppl. **5,** 395–398 (2004).
4. P. Cinzano, "Modelling light pollution from searchlights," Mem. Soc. Astron. Ital. **71,** 239–250 (2000).
5. K. Sokanský, "Výskum emisí světelného rušení vyvolaného veřejným osvětlením za účelem jeho omezení v dopravě měst a obcí (The study of light pollution originated from public illumination and its relation to traffic concentration in cities and villages)," Grant MMR: WB-23-05, Fakulta elektrotechniky a informatiky, VŠB-TU Ostrava Czech Republic (2005–2006).
6. P. Cinzano, F. Falchi, and C. D. Elvidge, "The first world atlas of the artificial night sky brightness," Mon. Notes Astron. Soc. **328,** 689–707 (2001).
7. D. X. Kerola, "Modelling artificial night-sky brightness with a polarized multiple scattering radiative transfer computer code," Mon. Notes Astron. Soc. **365,** 1295–1299 (2006).
8. J. H. Joseph, Y. J. Kaufman, and Y. Mekler, "Urban light

pollution: the effect of atmospheric aerosols on astronomical observations at night," Appl. Opt. **30,** 3047–3058 (2001).
9. M. Kocifaj and J. Lukáč, "Using the multiple scattering theory for calculation of the radiation fluxes from experimental aerosol data," J. Quant. Spectrosc. Radiat. Transfer **60,** 933–942 (1998).
10. H. C. Van de Hulst, *Multiple Light scattering. Tables, Formulas and Applications* (Academic, 1980).
11. E. J. McCartney, *Optics of the Atmosphere* (Wiley, 1977).
12. G. P. Gushchin, *The Methods, Instrumentation and Results of Atmospheric Spectral Measurements* (Gidrometeoizdat, 1988), in Russian.
13. M. I. Mishchenko, L. D. Travis, and A. A. Lacis, *Scattering, Absorption, and Emission of Light by Small Particles* (Cambridge U. Press, 2002).
14. C. J. Braak, J. F. de Haan, C. V. M. Van der Mee, J. W. Hovenier, and L. D. Travis, "Parameterized scattering matrices for small particles in planetary atmospheres," J. Quant. Spectrosc. Radiat. Transfer **69,** 585–604 (2001).
15. C. Levoni, E. Cattani, M. Cervino, R. Guzzi, and W. D. Nicolantonio, "Effectiveness of the MS-method for computation of the intensity field reflected by a multi-layer plane parallel atmosphere," J. Quant. Spectrosc. Radiat. Transfer **69,** 635–650 (2001).
16. O. V. Kalashnikova and I. N. Sokolik, "Modeling the radiative properties of nonspherical soil-derived mineral aerosols," J. Quant. Spectrosc. Radiat. Transfer **87,** 137–166 (2004).
17. M. I. Mishchenko, J. M. Dlugach, E. G. Zanovitskij, and N. T. Yakharova, "Bidirectional reflectance of flat, optically thick particulate layers: an efficient radiative transfer solution and applications to snow and soil surfaces," J. Quant. Spectrosc. Rad. Transfer **63,** 409–432 (1999).
18. D. Lubin and P. G. Weber, "The use of cloud reflectance functions with satellite data for surface radiation budget estimation," J. Appl. Meteorol. **34,** 1333–1347 (1995).
19. R. H. Garstang, "Model for artificial night-sky illumination," Astron. Soc. Pac. Pub. **98,** 364–375 (1986).
20. R. H. Garstang, "Night-sky brightness at observatories and sites," Astron. Soc. Pac. Pub. **101,** 306–329 (1989).
21. *International Lighting Vocabulary* (CIE No. 17.4, 1987).
22. A. Barducci, D. Guzzi, P. Marcoionni, and I. Pippi, "Algorithm for the retrieval of columnar water vapor from hyperspectral remotely sensed data," Appl. Opt. **43,** 5552–5563 (2004).
23. L. M. Celnikier, "Understanding the physics of meteoritic descent," Am. J. Phys. **63,** 524–535 (1995).
24. A. A. Kokhanovsky, V. V. Rozanov, E. P. Zege, H. Bovensmann, and J. P. Burrows, "A semianalytical cloud retrieval algorithm using backscattered radiation in 0.4–2.4 μm spectral region," J. Geophys. Res. D **108** (D1), doi:10.1029/2001JD001543 (2003).
25. I. N. Minin, *Theory of Radiative Transfer in Planetary Atmospheres* (Nauka, 1988), in Russian.
26. R. N. Green, B. A. Wielicki, J. A. Coakley, L. L. Stowe, P. O'R. Hinton, and Y. Hu, "Clouds and the Earth's radiant energy system (CERES) algorithm theoretical basis document," CERES Inversion to Instantaneous TOA Fluxes, Release 2.2, June 2 (NASA, 1997).
27. N. C. Hsu, "Radiative impacts from biomass burning in the presence of clouds during boreal spring in southeast Asia," Geophys. Res. Lett. **30,** doi:10.1029/2002GL016485 (2003).
28. W. O'Hirok and C. Gautier, "Potential biases in remotely sensed cloud properties due to the plane parallel cloud assumption employed in retrieval algorithms," in Proc. SPIE **3867,** 8–16 (1999).
29. M. Kocifaj, "Scattered light in urban areas and its angular behavior influenced by complex morphology of dust-like aerosols)," Grant APVV-0112-06, Slovak Academy of Sciences, Slovak Republic (2006).